JOURNAL OF GEOPHYSICAL RESEARCH, VOL. 102, NO. D14, PAGES 16,593–16,603, JULY 27, 1997

Comparison of the seasonal change in cloud-radiative forcing from atmospheric general circulation models and satellite observations

R. D. Cess,[1] M. H. Zhang,[1] G. L. Potter,[2] V. Alekseev,[3] H. W. Barker,[4] S. Bony,[5] R. A. Colman,[6] D. A. Dazlich,[7] A. D. Del Genio,[8] M. Déqué,[9] M. R. Dix,[10] V. Dymnikov,[3] M. Esch,[11] L. D. Fowler,[7] J. R. Fraser,[6] V. Galin,[3] W. L. Gates,[2] J. J. Hack,[12] W. J. Ingram,[13] J. T. Kiehl,[12] Y. Kim,[8] H. Le Treut,[5] X.-Z. Liang,[14] B. J. McAvaney,[6] V. P. Meleshko,[15] J. J. Morcrette,[16] D. A. Randall,[7] E. Roeckner,[11] M. E. Schlesinger,[17] P. V. Sporyshev,[15] K. E. Taylor,[2] B. Timbal,[9] E. M. Volodin,[3] W. Wang,[17] W. C. Wang,[14] and R. T. Wetherald[18]

Abstract. We compare seasonal changes in cloud-radiative forcing (CRF) at the top of the atmosphere from 18 atmospheric general circulation models, and observations from the Earth Radiation Budget Experiment (ERBE). To enhance the CRF signal and suppress interannual variability, we consider only zonal mean quantities for which the extreme months (January and July), as well as the northern and southern hemispheres, have been differenced. Since seasonal variations of the shortwave component of CRF are caused by seasonal changes in both cloudiness and solar irradiance, the latter was removed. In the ERBE data, seasonal changes in CRF are driven primarily by changes in cloud amount. The same conclusion applies to the models. The shortwave component of seasonal CRF is a measure of changes in cloud amount at all altitudes, while the longwave component is more a measure of upper level clouds. Thus important insights into seasonal cloud amount variations of the models have been obtained by comparing both components, as generated by the models, with the satellite data. For example, in 10 of the 18 models the seasonal oscillations of zonal cloud patterns extend too far poleward by one latitudinal grid.

[1]Institute for Terrestrial and Planetary Atmospheres, Marine Sciences Research Center, State University of New York at Stony Brook.
[2]Program for Climate Model Diagnosis and Intercomparison, Lawrence Livermore National Laboratory, Livermore, California.
[3]Department of Numerical Mathematics, Russian Academy of Sciences, Moscow.
[4]Canadian Climate Centre, Downsview, Ontario.
[5]Laboratoire de Météorologie Dynamique, Paris.
[6]Bureau of Meteorology Research Centre, Melbourne, Victoria, Australia.
[7]Department of Atmospheric Science, Colorado State University, Fort Collins.
[8]NASA Goddard Institute for Space Studies, New York.
[9]Météo-France, Centre National de Recherches Météorologiques, Toulouse, France.
[10]Division of Atmospheric Research, Commonwealth Scientific and Industrial Research Organisation, Aspendale, Victoria, Australia.
[11]Max Planck Institute for Meteorology, Hamburg, Germany.
[12]National Center for Atmospheric Research, Boulder, Colorado.
[13]Hadley Centre for Climate Prediction and Research, U. K. Meteorological Office, Bracknell, England.
[14]Atmospheric Sciences Research Center, State University of New York at Albany.
[15]Voeikov Main Geophysical Obseratory, St. Petersburg, Russia.
[16]European Centre for Medium-Range Weather Forecasts, Reading, England.
[17]Department of Atmospheric Sciences, University of Illinois, Urbana.
[18]Geophysical Fluid Dynamics Laboratory, National Oceanic and Atmospheric Administration, Princeton University, Princeton, New Jersey.

Copyright 1997 by the American Geophysical Union.

Paper number 97JD00927.
0148-0227/97/97JD-00927$09.00

1. Introduction

Three-dimensional general circulation models (GCMs) are the most comprehensive climate models for projecting climate change caused by human activities. One of the greatest uncertainties associated with these models, however, is their ability to simulate how climate-induced changes in cloudiness will impact a climate change projection; i.e., cloud feedback in which cloudiness changes might amplify (positive feedback) or diminish (negative feedback) a model's simulated climate change. A broad range of cloud feedbacks was noted in a comparison of 19 atmospheric GCMs [*Cess et al.*, 1990], while a more recent comparison [*Cess et al.*, 1996] showed a more narrow difference, with most models producing modest cloud feedback. There were, however, substantial differences in the longwave and shortwave feedback components, indicating that the models still have physical disagreements. Clearly, there is a need to improve our understanding of cloud-climate interactions. Although not an analog for long-term climate change, seasonal variations of cloud-radiative forcing constitute one means of testing cloud-climate interactions in GCMs and, perhaps more importantly, of providing physical insights into such interactions.

In this study, 18 atmospheric GCMs are compared with seasonal variations of cloud-radiative forcing as determined from Earth Radiation Budget Experiment (ERBE) satellite data. Seasonal variations of the shortwave component are driven by seasonal changes in both cloudiness and solar irradiance, and the latter is removed so as to isolate the impact of cloudiness variations. The goal of this particular comparison is to demonstrate what can be learned by comparing a number of

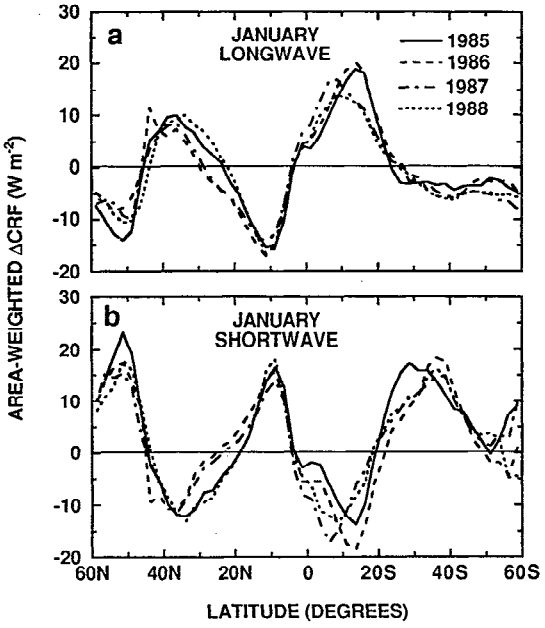

Figure 1. Zonal mean and area-weighted (a) LW and (b) SW ΔCRF for January of each of the 4 years (1985 to 1988).

GCMs with seasonal cloud-radiative forcing data; it is not to determine which models are the "best models." Models that may be superior to others when compared with seasonal cloud-radiative forcing data might not show similar superiority when compared with other types of data.

2. Seasonal Cloud-Radiative Forcing

The term "cloudy" is used to denote a domain containing both overcast-sky and clear-sky regions, following *Ramanathan et al.* [1989], while the term clear refers to an average of clear-sky regions within that domain. We employ monthly mean top-of-the-atmosphere (TOA) reflected shortwave (SW) and emitted longwave (LW) radiative fluxes as provided by the ERBE for 2.5° longitude and 2.5° latitude grids and for both cloudy and clear designations [*Ramanathan et al.*, 1989; *Harrison et al.*, 1990]. With H representing the net TOA radiative heating of the climate system

$$H = (1 - \alpha)S - F \tag{1}$$

where α, S, and F denote the albedo, solar irradiance, and emitted LW radiation at the TOA, respectively. Cloud-radiative forcing (CRF) refers the cloudy-sky H to that for clear skies, so that [*Ramanathan et al.*, 1989]

$$\text{CRF} = (\alpha_c - \alpha)S + (F_c - F) \tag{2}$$

where the subscript c is used to denote clear-sky quantities. Positive values of CRF indicate that clouds radiatively heat the climate system, while negative values correspond to cooling. Since $(F_c - F)$ is generally positive, this represents the LW greenhouse warming caused by clouds. Conversely, $(\alpha_c - \alpha)$ is generally negative, and so the first term in (2) is a cooling due to SW reflection by clouds.

To investigate the seasonal variation of CRF, we follow *Cess et al.* [1992a] and let Δ denote the seasonal variation of a given quantity about its annual mean value which is denoted by an overbar (e.g., $\Delta S = S - \bar{S}$). The evaluation of the LW component of ΔCRF is straightforward, giving

$$\text{LW } \Delta\text{CRF} = \Delta F_c - \Delta F \tag{3}$$

while for the SW component

$$\text{SW } \Delta\text{CRF} = (\bar{\alpha}_c - \bar{\alpha})\Delta S + (\Delta\alpha_c - \Delta\alpha)S + (\bar{S}\bar{\alpha}_c - \bar{S}\bar{\alpha} - \overline{S\alpha_c} + \overline{S\alpha})$$

It is important to recognize that averaging is performed on fluxes and not albedos, so that the definitions of $\bar{\alpha}$ and $\bar{\alpha}_c$ follow from $\bar{\alpha}\bar{S} = \overline{\alpha S}$ and $\bar{\alpha}_c\bar{S} = \overline{\alpha_c S}$. Thus the above expression reduces to

$$\text{SW } \Delta\text{CRF} = (\bar{\alpha}_c - \bar{\alpha})\Delta S + (\Delta\alpha_c - \Delta\alpha)S \tag{4}$$

The first term in (4) is related solely to seasonal variability of the solar irradiance and contains no information concerning seasonal cloudiness variability. Thus we delete this term and define the SW ΔCRF as [*Cess et al.*, 1992a]

$$\text{SW } \Delta\text{CRF} = (\Delta\alpha_c - \Delta\alpha)S \tag{5}$$

Note that S represents the monthly mean solar irradiance for the month in question, rather than the annual mean solar irradiance $\bar{S}$.

All quantities in (3) and (5) are available from the ERBE monthly mean processed data [*Harrison et al.*, 1990]. The conventional data set consists of roughly 2 initial years of combined data from the Earth Radiation Budget Satellite (ERBS) which was in a 57° orbit relative to the equator, and NOAA 9, whose orbit was Sun synchronous with a 1430 LT equator crossing time. The NOAA 9 scanner failed about 2 months after the launch of NOAA 10, whose orbit was also Sun synchronous but with an 0730 LT equator crossing time. So there are roughly two months of combined data from ERBS, NOAA 9, and NOAA 10, followed by about 2 years of combined data from ERBS and NOAA 10, at which time the NOAA 10 scanner failed. The last (fifth) year of data is solely from ERBS. All this raises the possibility of artificial "interannual variability" caused by changes in satellite combinations. To avoid this, we employ data solely from ERBS. This imposes a restriction to latitudes less than 60° as dictated by the ERBS orbit. However, even if this were not the case, the ERBE clear-sky scene identification is not reliable over snow and ice [*Nemesure et al.*, 1994], so that high latitudes should be excluded.

Regional plots of ΔCRF exhibit substantial interannual variability, a problem that is reduced by addressing only zonal mean ΔCRF. However, care must be exercised in performing the zonal averaging because of missing clear-sky grid points that are due to cloudiness persisting over some regions throughout an entire month. This will result in missing ΔCRF values for those grid points, so that if ΔCRF is zonally averaged, the missing grids result in biases because those grids contain large amounts of clouds. A more accurate procedure is to first evaluate zonal means of F and α, noting for the latter case that averaging the albedo is equivalent to averaging the flux because the monthly mean TOA insolation is effectively constant in the zonal direction. Unlike the clear quantities, there are no missing grid values. Next, F_c and α_c are zonally averaged with missing clear-sky grids not being counted in either the numerator or denominator when performing the averaging. This removes the aforementioned bias associated with averaging ΔCRF, because enhanced cloudiness over the missing clear-sky grid points would not bias the clear-sky averages. Zonal averages of LW and SW ΔCRF are then evaluated from (3) and (5) using the zonal mean input.

To be consistent with the GCM simulations, as will be discussed in the following section, only 4 of the 5 years of ERBE data are used, 1985 through 1988. January LW and SW ΔCRF results for each of these years are shown in Figure 1a and 1b, respectively. The ΔCRF values have been weighted by latitudinal area through multiplication by the cosine of latitude. The latitudinal variations of LW and SW ΔCRF are the result of seasonal shifts of cloudiness with latitude. The features that dominate tropical latitudes are caused by the migration of the intertropical convergence zone (ITCZ), relative to the annual mean, into the summer hemisphere. This migration of enhanced cloudiness is responsible for the respective positive and negative peaks in LW and SW ΔCRF at roughly latitude 10°S.

There are two important points to note concerning Figure 1. The interannual variability is substantial, even after zonal averaging has been performed, and the magnitude of the zonal signals are small, roughly 20 W m^{-2}. Differencing the extreme months (January minus July) and the southern and northern hemispheres (SH minus NH) amplifies the signal and suppresses interannual variability, as Figures 2a and 2b show. This double differencing is adopted for comparison with the GCMs. The January minus July differencing clearly represents a seasonal change, while the SH minus NH differencing is to some extent an amplification of the seasonal change because of the reversal of seasons. The maximum signals, roughly 60 W m^{-2}, are well above the ±5.5 W m^{-2} (SW) and ±3.2 W m^{-2} (LW) uncertainties in the ERBE monthly mean regional data [*Wielicki et al.*, 1995], and these uncertainties should be even less in the double-differenced zonal mean data we have adopted.

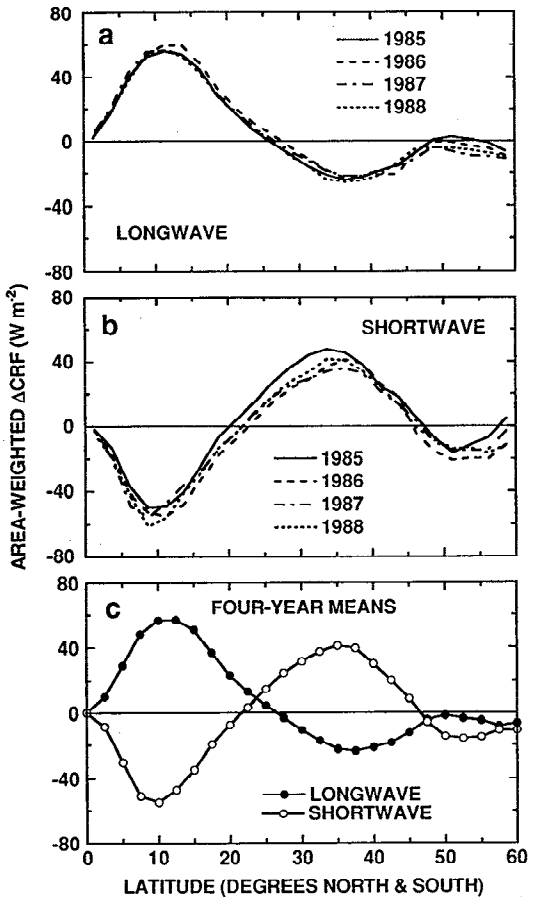

Figure 2. (a) Zonal-mean and area-weighted January minus July and SH minus NH LW ΔCRF for each of the 4 years. (b) The same as Figure 2a but for the SW. (c) Four-year means of the LW ΔCRF from Figure 2a and the SW ΔCRF from Figure 2b.

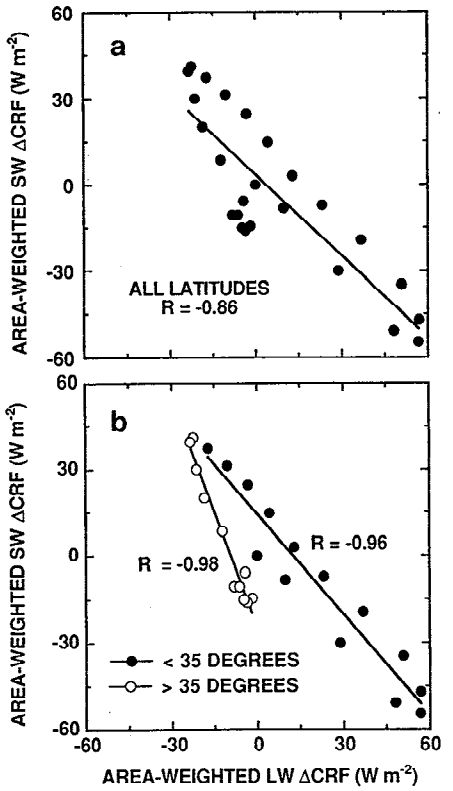

Figure 3. Scatterplots of the SW ΔCRF versus LW ΔCRF results shown in Figure 2c, (a) for all latitudes and (b) subdivided at latitude 35°. *R* denotes the correlation coefficient.

The strong anticorrelation between LW and SW ΔCRF (Figure 2c) suggests that both are governed primarily by seasonal changes in cloud amount. An increase in cloud amount, such as the migration of the ITCZ into the summer hemisphere, simultaneously increases LW ΔCRF and decreases SW ΔCRF. Figure 3a clearly demonstrates this anticorrelation. Each point represents the SW and LW ΔCRF pairs, for 2.5° latitude zones, from Figure 2c. This correlation is considerably increased when the data are separated for latitudes below and above 35°, as shown in Figure 3b. Thus with one exception that will be discussed later, ΔCRF serves mainly as a measure of seasonal changes in cloud amount.

There are, however, two caveats that apply to the discussion above. Correlated opposite-sign changes in SW and LW ΔCRF could be caused by changes in cirrus optical depth because the emissivity of cirrus clouds is generally less than unity. An increase in cirrus optical depth would thus increase the magnitudes of both SW and LW ΔCRF. Moreover, LW ΔCRF deduced by ERBE depends also on changes in cirrus structure. For example, if the degree of horizontal variability of two cirrus clouds differed, but cloud fraction and optical depth were equal, the scenes could still yield significantly different values of LW CRF [*Barker et al.*, 1993]. Since GCMs assume that all clouds are homogeneous, and therefore overlook changes to LW CRF due to changes in cloud structure, it may at times be incorrect to attribute differences between GCM and ERBE values of LW ΔCRF simply to differences in cloud fraction.

Table 1. List of GCMs Used in the Present Study

Model	Investigators
Bureau of Meteorology Research Centre, (BMRC)	McAvaney, Fraser, Colman
Canadian Climate Centre (CCC)	Barker
NCAR Community Climate Model, Version 2 (CCM2, CCM2A)	Kiehl, Hack, Zhang, Cess
NCAR Community Climate Model, Version 1; Lawrence Livermore National Laboratory (CCM/LLNL)	Taylor
Centre National de Recherches Météorologiques (CNRM)	Timbal and Déqué
Commonwealth Scientific and Industrial Research Organisation (CSIRO)	Dix
Colorado State University (CSU 95)	Randall, Dazlich, Fowler
Department of Numerical Mathematics of the Russian Academy of Sciences (DNM)	Galin, Dymnikov, Volodin, Alekseev
GENESIS/State University of New York at Albany	Liang and W. C. Wang
Max Planck Institute for Meteorology Hamburg (ECHAM)	Roeckner and Esch
European Centre for Medium-Range Weather Forecasts, Cycle 36 (ECMWF)	Morcrette, Potter, Gates
Geophysical Fluid Dynamics Laboratory (GFDL)	Wetherald
NASA Goddard Institute for Space Studies (GISS)	Del Genio and Kim
Laboratoire de Météorologie Dynamique (LMD)	Bony and Le Treut
Main Geophysical Observatory (MGO)	Meleshko and Sporyshev
University of Illinois at Urbana-Champagne (UIUC)	Schlesinger and W. Wang
Hadley Centre for Climate Prediction and Research, United Kingdom Meteorological Office (UKMO)	Ingram

3. GCM Simulations

The GCMs used in the present study are summarized in Table 1, and descriptions of most of these models are provided by *Phillips* [1994], although in many instances the models have since been updated. Two versions of CCM2 have been used, the standard version (CCM2), and a modified version (CCM2A) in which cloud SW absorption was increased as suggested by some recent observationally based studies [*Ramanathan et al.*, 1995; *Cess et al.*, 1995; *Pilewskie and Valero*, 1995] by modifying the cloud single-scattering albedo as described by *Kiehl et al.* [1995]. The model-generated LW and SW ΔCRF were from the last 4 years (1985–1988) of 10-year simulations performed as part of the Atmospheric Model Intercomparison Project (AMIP), which used prescribed seasonally varying sea surface temperatures over the 10-year period [*Gates*, 1992]. For the purpose of comparing the GCM results to ERBE, the ERBE LW and SW ΔCRF were interpolated to the latitudinal grids of each GCM by using a cubic spline interpolation.

The procedure for calculating LW and SW ΔCRF is the same as has been described for the ERBE data, except for the clear-sky fluxes. Method II [*Cess and Potter*, 1987] was adopted for the clear-sky flux evaluation, by which the clear fluxes are diagnostically evaluated at each grid by setting cloud amount to zero. Therefore there are no missing clear-sky grid points in the models. This sampling discrepancy between the models and the ERBE data could impact the interpretation of ΔCRF. Several studies have been conducted to examine alternate sampling methods in models and their impact on CRF [*Cess et al.*, 1992b; *Potter et al.*, 1992; *Zhang et al.*, 1994; *Barker*, 1995]. It can be concluded from these studies that although Method II can produce a clear-sky bias in CRF for some regions, this sampling discrepancy has negligible impact on zonal mean ΔCRF, largely because the biases cancel when taking the difference in monthly mean and annual mean CRF to obtain ΔCRF.

4. Model-Data Comparisons

Summarized in Figure 4 are model versus ERBE comparisons of LW ΔCRF (Figure 4a), SW ΔCRF (Figure 4b), and net ΔCRF (Figure 4c), which is the sum of the LW and SW components. The same information is summarized in Figure 5 in the form of GCM versus ERBE differences, and the root-mean-square (RMS) of these differences are shown in Figure 6 for each model. In general, with this sign convention the models tend to underestimate LW ΔCRF in the tropics and overestimate it in midlatitudes (Figure 5a). Only CSU 95 and GENESIS produce positive differences from ERBE through-

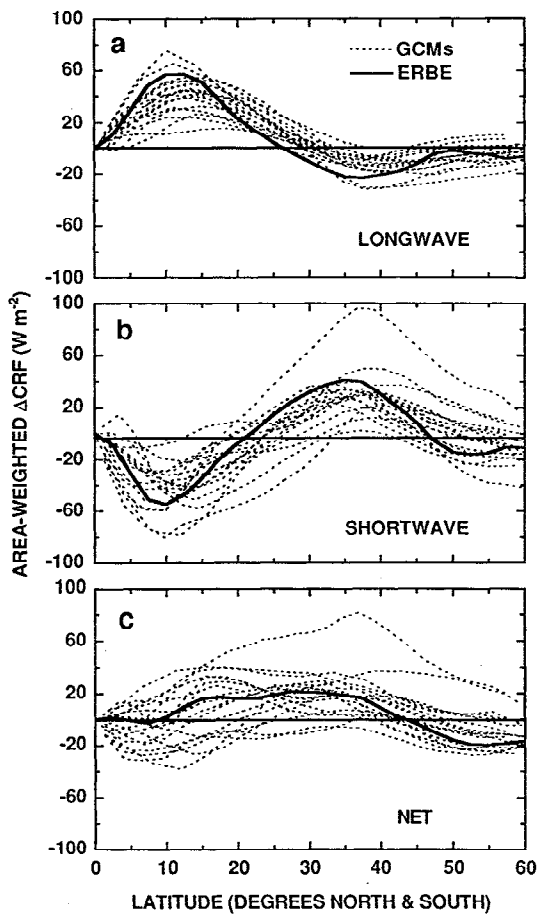

Figure 4. The Zonal mean (a) LW, (b) SW, and (c) net (LW + SW) ΔCRF for the 18 GCMs compared with that for ERBE.

out the tropics. Because the ERBE LW and SW ΔCRF are primarily driven by seasonal variations in cloud amount and thus are anticorrelated, one might anticipate that the SW ΔCRF differences from ERBE should exhibit similar behavior, with the sign reversed, to those for LW ΔCRF, Figure 5b shows evidence of this. Also, if the GCM versus ERBE differences were caused mainly by models producing errors in the seasonal variability of cloud amount, then because the errors in LW and SW ΔCRF would be of opposite sign, one might expect that the net ΔCRF would exhibit better agreement than for the LW and SW components because of partial compensation of the component errors. Figure 5c illustrates, however, that this is not the case, as will later be addressed.

To better understand what is happening, note from Figure 6 that only CNRM, CSIRO, CSU 95, and UIUC produce SW RMS differences smaller than those for the LW; for most models the greatest RMS difference is that of the SW. It might be tempting to conclude that the reason for most models producing greater SW differences is that greater uncertainty should be associated with the models' SW cloud reflectances than with their LW emittances. However, the real explanation appears to be more subtle. In the previous section we emphasized that both LW and SW ΔCRF are primarily driven by seasonal cloud amount variations, but there is a caveat to this. Low level clouds provide a minimal contribution to LW ΔCRF, while they are significant contributors to SW ΔCRF. Thus if a model contained significant errors in seasonal changes in low level clouds, this would contribute to errors in SW ΔCRF but not in LW ΔCRF. The point is that SW ΔCRF is influenced by all clouds, whereas LW ΔCRF is strongly dependent upon upper level clouds. Further discussion of this is given in the following section.

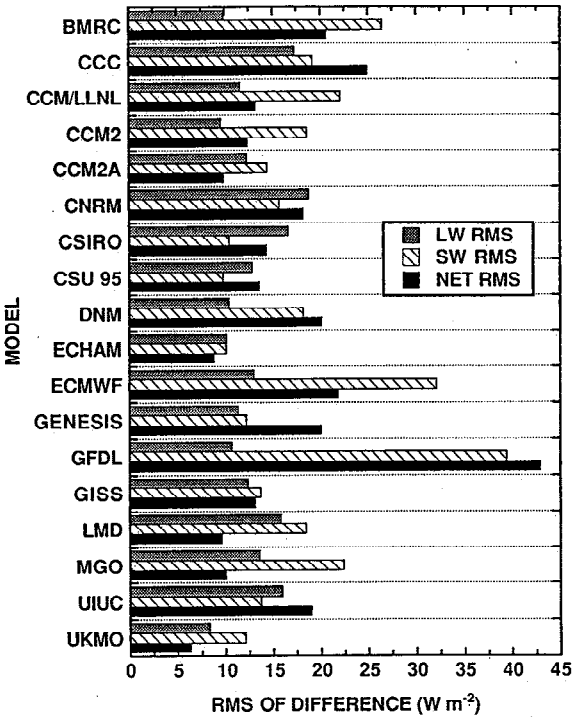

Figure 6. Summary of the root-mean-square (RMS) of the GCM minus ERBE differences shown in Figure 5.

At least part of the LW ΔCRF differences shown in Figures 5a and 6 can be attributed to a systematic error present in 10 of the models. To demonstrate this, we select two models for which this error is minimal (CSU 95 and UKMO) and two for which it is not (MGO and LMD). Figure 7a compares LW

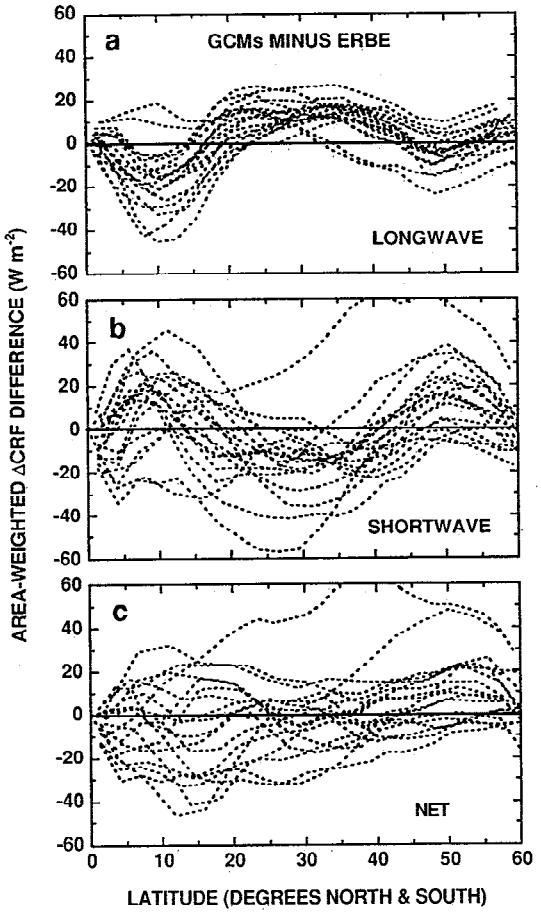

Figure 5. GCM minus ERBE differences in zonal mean (a) LW, (b) SW, and (c) net ΔCRF.

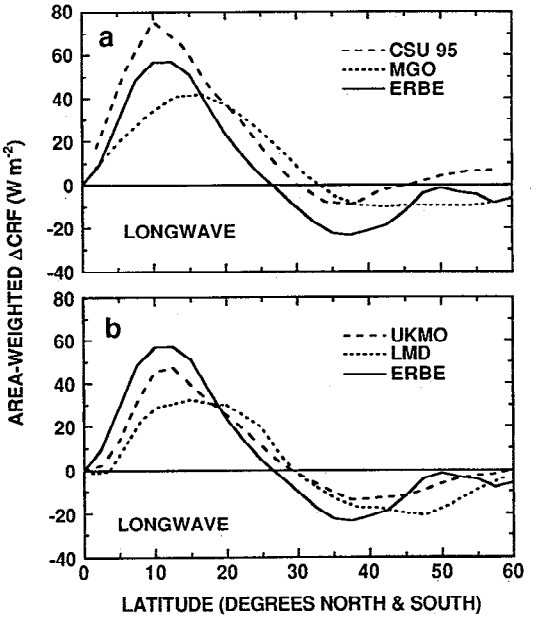

Figure 7. Zonal-mean LW ΔCRF for (a) CSU 95, MGO, and ERBE and for (b) UKMO, LMD, and ERBE.

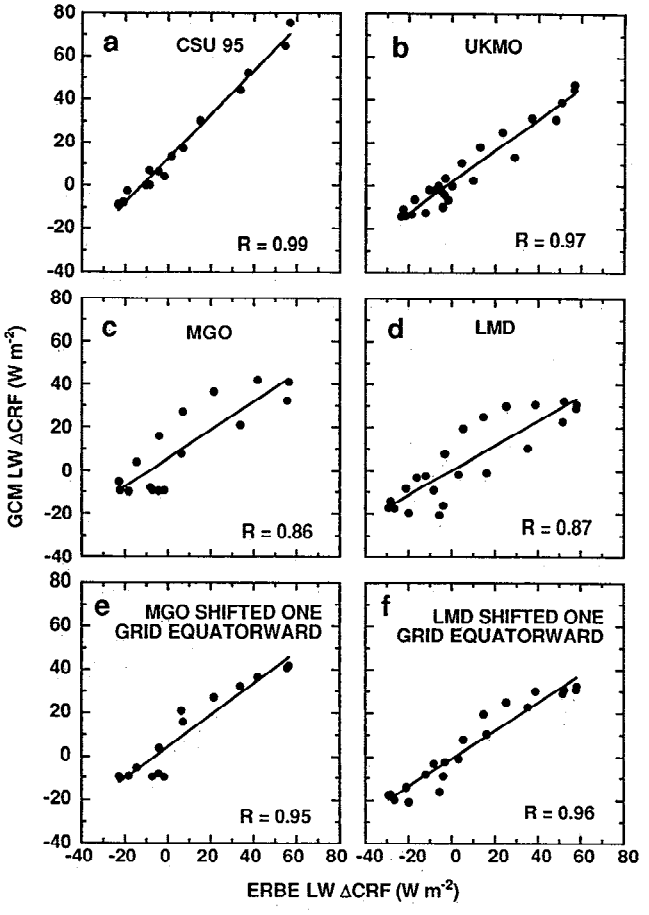

Figure 8. (a) Scatterplot of the zonal mean LW ΔCRF for CSU 95 versus that for ERBE. (b) The same as Figure 8a but for UKMO. (c) The same as Figure 8a but for MGO. (d) The same as Figure 8a but for LMD. (e) The same as Figure 8c but for the MGO LW ΔCRF shifted one grid equatorward. (f) The same as Figure 8d but for LMD LW ΔCRF shifted one grid equatorward.

ΔCRF for CSU 95 and MGO to ERBE. Note that for CSU 95 the latitudinal location of the tropical peak is correct, whereas for MGO the peak is located at a higher latitude. Similar conclusions apply to UKMO (proper location) and LMD (higher latitude location) as shown in Figure 7b. As was previously discussed, this peak is associated with the poleward migration of the ITCZ into the summer hemisphere, so the implication is that both MGO and LMD, plus eight other models, produce a seasonal oscillation of the ITCZ that extends too far poleward.

An alternate way of demonstrating this is to plot the models' LW ΔCRF against that for ERBE, as shown in Figures 8a through 8d. Here the emphasis is on latitudinal phasing errors which are appropriately measured by the correlation coefficient R, whereas the RMS of the difference additionally includes errors in amplitude. High correlations are exhibited by CSU 95 (Figure 8a) and UKMO (Figure 8b), because of their realistic portrayals of the latitudinal phase of the ERBE LW ΔCRF (Figure 7), whereas MGO (Figure 8c) and LMD (Figure 8d) exhibit "hysteresis loops" caused by their phasing errors, and 10 of the models exhibit this behavior to varying degrees. What is interesting is that for all 10 models the GCM versus ERBE LW ΔCRF correlation coefficient is maximized by shifting the GCM ΔCRF equatorward by one latitudinal grid. Shifted correlations are illustrated in Figure 8e for MGO and in Figure 8f for LMD. The remaining eight models do not exhibit this behavior; an equatorward shift produces a decrease in correlation, and no model exhibits an increase in correlation for a poleward shift.

The increases in LW correlation coefficient, as a consequence of the equatorward shift in ΔCRF, are summarized in Figure 9a for the 10 models that exhibit this behavior. These include all the models employing moisture convergence as the closure in their convection schemes (BMRC, CNRM, ECHAM, ECMWF, LMD, and MGO). With three exceptions, these models exhibit an increase in the SW correlation coefficient when ΔCRF is shifted one grid equatorward, as is shown in Figure 9b. This simultaneous increase in both correlation coefficients is consistent with a latitudinal phasing error in cloudiness which would influence both LW and SW ΔCRF. The exceptions are CNRM, CSIRO, and ECHAM, which show small reductions in their SW correlation coefficients. Like MGO and LMD (Figure 7), CSIRO exhibits a poleward shift of the tropical LW ΔCRF feature as shown in Figure 10a, but Figure 10b demonstrates that while a comparable shift occurs in the tropical SW feature, there is no apparent SW phasing error at midlatitudes, where the SW feature is more pronounced than that of the LW. Thus while a poleward shift in

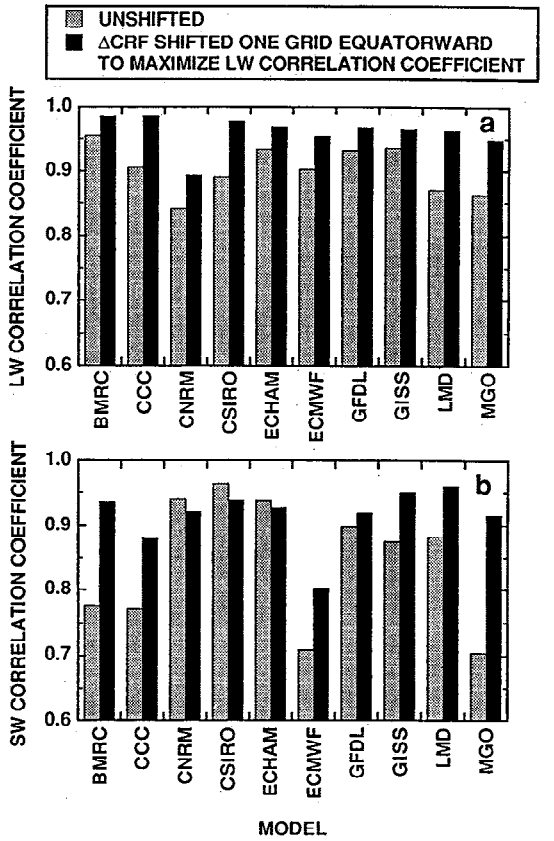

Figure 9. Summary of the (a) LW and (b) SW correlation coefficient, evaluated from scatterplots as in Figure 8, for the ten models that exhibit the latitudinal phasing error. These are for no latitudinal shift of ΔCRF, and for a one-grid equatorward shift of ΔCRF that maximizes the LW correlation coefficient. Note that the equatorward shift refers to maximizing the LW R and not the SW R.

SW ΔCRF minimizes the tropical phasing error, it actually introduces a phasing error at midlatitudes, giving a small decrease in the SW correlation coefficient overall. While ECHAM likewise has a smaller shifted SW correlation coefficient, it is for quite different reasons. This model exhibits a poleward shift in LW ΔCRF for both the tropics and midlatitudes (Figure 10c), with a comparable shift in SW ΔCRF at midlatitudes but not in the tropics (Figure 10d). Thus while for both models the equatorward shift of ΔCRF produces an increase in the LW correlation coefficient and a decrease in the SW correlation coefficient, the causes are not the same.

5. Selected Model-Data Interpretations

Three models serve to illustrate the reasons (but not the causes) of the model-ERBE differences shown in Figure 5; these are CSIRO, ECHAM, and GFDL. Their LW and SW RMS of the differences, given in Figure 6, are shown again in Figure 11. CSIRO and ECHAM have nearly identical, and quite modest, SW values, while CSIRO has one of the larger LW values. Conversely, ECHAM and GFDL have virtually identical, and also modest, LW values, but GFDL has the largest SW value. To understand the reasons for this, LW and SW ΔCRF for these models, as a function of latitude, are shown in Figure 12. As for the ERBE data (see Figure 2c), the models exhibit strong anticorrelation of the LW and SW components, indicating that like the ERBE data, ΔCRF is principally driven by seasonal changes in cloud amount. Recall, however, that SW ΔCRF is influenced by all clouds, whereas LW ΔCRF is strongly dependent upon upper level clouds, and this serves to account for most of the model-to-model differences shown in Figures 11 and 12, as well as the model versus ERBE differences that are summarized in Figure 13. Note from Figures 13a and 13b that CSIRO and ECHAM produce similar departures from ERBE in the extratropics. It is in the tropics

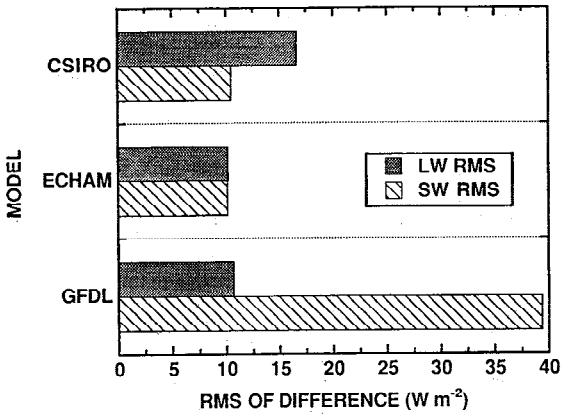

Figure 11. Summary of the RMS of the LW and SW ΔCRF GCM versus ERBE differences fir CSIRO, ECHAM and GFDL. These same values are shown in Figure 6.

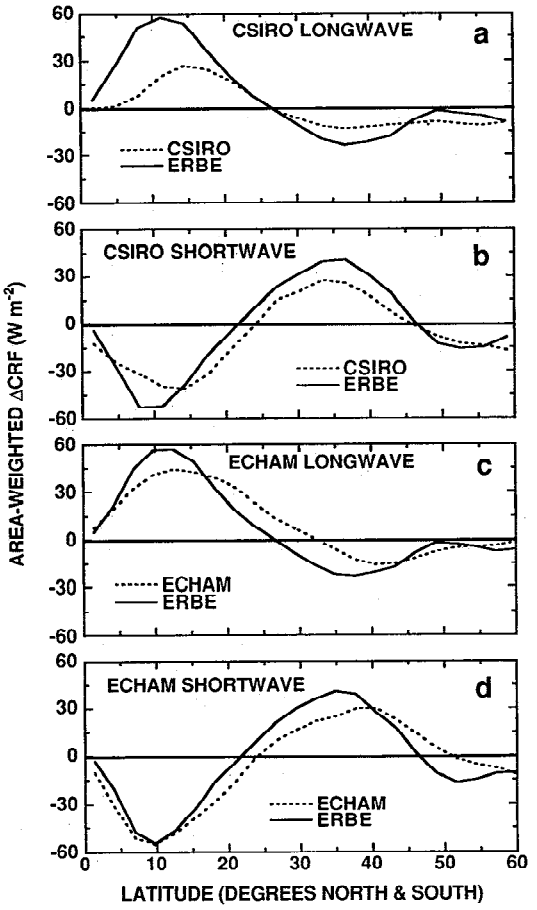

Figure 10. (a) Zonal mean LW ΔCRF for CSIRO (unshifted) and ERBE. (b) Same as Figure 10a but for the SW. (c) Same as Figure 10a but for ECHAM. (d) Same as Figure 10b but for ECHAM.

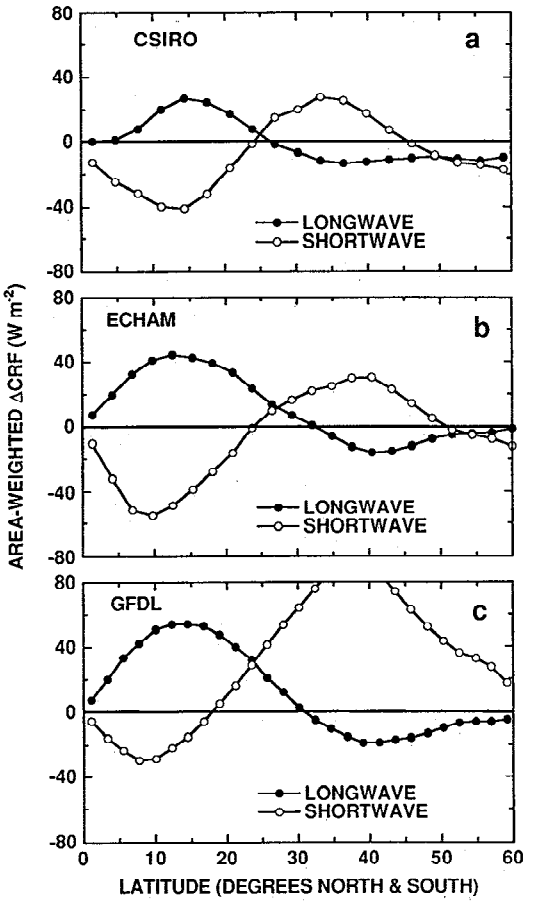

Figure 12. Zonal mean LW and SW ΔCRF for (a) CSIRO, (b) ECHAM, and (c) GFDL.

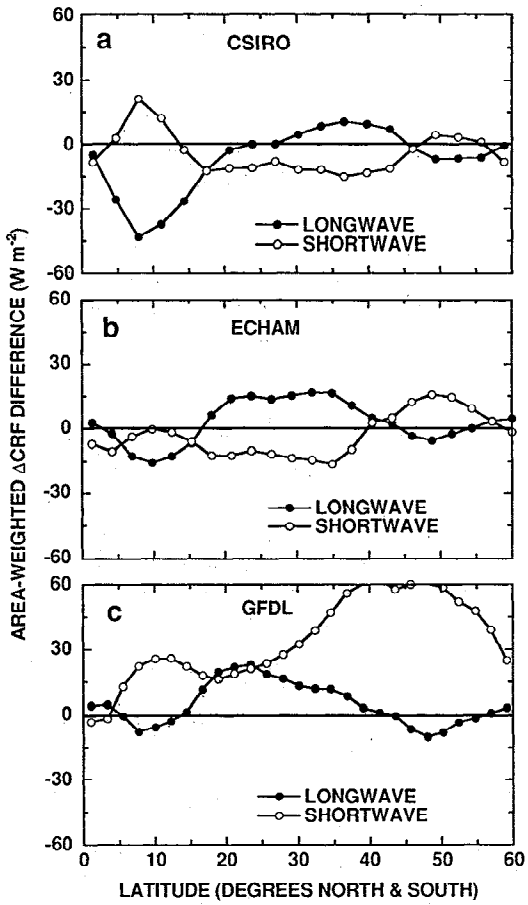

Figure 13. Zonal mean (a) CSIRO versus ERBE, (b) ECHAM versus ERBE, and (c) GFDL versus ERBE differences in LW and SW ΔCRF.

where CSIRO produces larger differences from ERBE, with the CSIRO LW ΔCRF magnitude being larger than that of the SW. This is the signature of upper level clouds, which produce greater LW than SW CRF, and thus greater LW than SW ΔCRF. So the primary difference between CSIRO and ECHAM is that CSIRO is producing larger errors in the seasonal variation of the amount of tropical cirrus.

A quite different explanation, but again related to cloud type, applies to the comparison of ECHAM (Figure 13b) and GFDL (Figure 13c). While the LW ΔCRF differences from ERBE are quite similar for these two models, GFDL exhibits much larger SW differences at midlatitudes. This behavior prompted an investigation into the seasonal variation of cloud amounts for GFDL (R. T. Wetherald, private communication, 1995), which revealed that although the model produced realistic annual mean amounts of low-level clouds, as well as realistic annual mean SW CRF, the magnitude of the seasonal variation of that model's low level clouds was unrealistically large at midlatitudes. This explains the results shown in Figure 13c, because SW ΔCRF is driven by the seasonal variation of clouds at all levels, whereas LW ΔCRF is quite insensitive to low level clouds. High level clouds efficiently trap LW radiation, thus resulting in large LW CRF, whereas low level clouds, with cloud top temperatures that differ little from the surface temperature, produce minimal LW CRF [*Ramanathan et al.*, 1989].

Although CSIRO, ECHAM, and GFDL all exhibit the latitudinal phasing error discussed in the previous section, this is not a major source of the differences shown in Figure 13. The comparisons in Figure 14 demonstrate that the equatorward shift in ΔCRF by one latitudinal grid produces a fairly modest reduction, for these models, in the LW RMS of the difference. This is also the case for the SW RMS, and similar conclusions apply to the seven other models that exhibit the latitudinal phasing error. MGO produces the largest reduction in LW RMS (from 13.6 to 9.8 W m^{-2}), while for the SW RMS the largest reduction is produced by CCC (from 17.3 to 14.8 W m^{-2}). Thus while the phasing error is interesting and may impact other quantities, such as seasonal precipitation patterns, it is not the primary cause of the model versus ERBE differences shown in Figure 5. Instead, these differences are mainly caused by errors in the seasonal variation of cloudiness.

At this point it is useful to return to the issue raised in section 4. Specifically, if the GCM versus ERBE ΔCRF differences are caused mainly by the models producing errors in the seasonal variability of cloud amount, then because the errors in LW and SW ΔCRF are of opposite sign, one might expect that the net ΔCRF would exhibit better agreement than for the LW and SW components because of partial compensation of the component errors, in contrast to what is shown in Figures 5 and 6. As was previously discussed, however, SW ΔCRF is sensitive to low level clouds, while LW ΔCRF is not. A comparison of BMRC and GFDL serves to make this point. Both models exhibit similar and quite modest LW ΔCRF differences

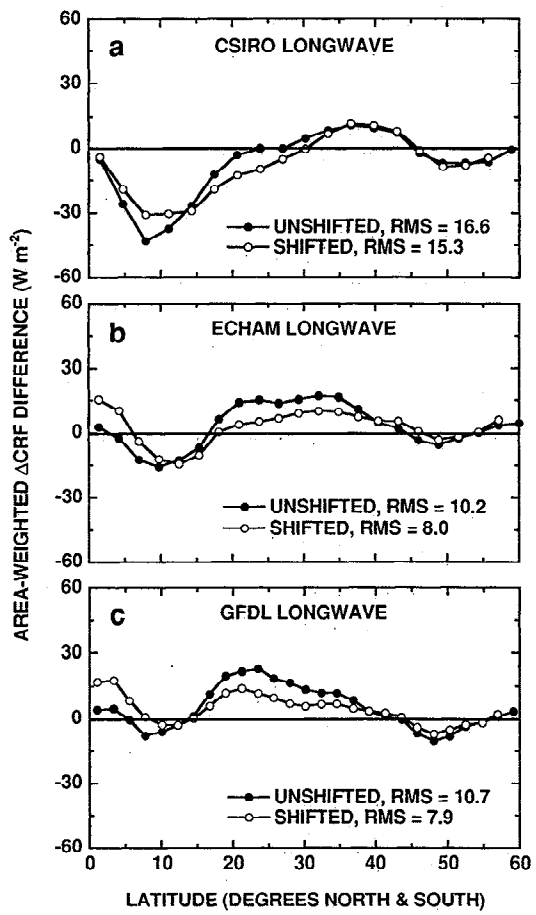

Figure 14. Zonal mean BMRC and GFDL versus ERBE differences in (a) LW ΔCRF, (b) SW ΔCRF, and (c) net ΔCRF.

relative to ERBE (Figure 15a), while their SW differences are quite different (Figure 15b). Those for GFDL have already been ascribed to an excessive magnitude of the seasonal variation of that model's low-level clouds, and the opposite sign of the SW differences for BMRC suggests possibly the reverse. In fact, the seasonality of the BMRC total cloud field is greater in amplitude than the International Satellite Cloud Climatology Project (ISCCP) observed values, although the overall pattern in the BMRC results tends to be shifted somewhat poleward. The negative SW ΔCRF difference for the BMRC results stems from two factors. The relative increase in summertime subtropical cloudiness is overdone and extends too far poleward (up to 32° latitude compared to 25° in the ISCPP results). As a result, the BMRC model produces "negative" SW ΔCRF over a wider range of these low latitudes. At higher latitudes the BMRC model substantially underestimates the "positive" SW ΔCRF that results from the relative decrease in summertime midlatitude cloudiness. Subsequent model runs have found this to be attributable mainly to the omission of any zenith angle dependent cloud albedo parameterization in this version of the model. In summary, the fact that the LW ΔCRF is quite similar for both models, and that both exhibit strong anticorrelation of LW and SW ΔCRF as demonstrated in Figure 12c for GFDL and in Figure 16 for BMRC, their differences from ERBE in SW ΔCRF are of opposite sign and this carries over to their net ΔCRF differences shown in Figure 15c.

Of particular interest are the comparisons of CCM2 and CCM2A shown in Figure 17. Some recent observations [*Ramanathan et al.*, 1995; *Cess et al.*, 1995; *Pilewskie and Valero*, 1995] suggest that cloud SW absorption may be far higher than normally modeled, and this was incorporated into CCM2A by reducing the cloud single-scattering albedos to reproduce the overall relationship between surface and TOA SW cloud forcing apparently shown by the observations. Since this change alone made the model much darker than satellite observations indicate, CCM2A was brought back into general agreement with observations by altering the critical relative humidities for cloud formation and other modifications. As is discussed by *Kiehl et al.* [1995], the impact of the inclusion of enhanced cloud absorption on the behavior of the model was dramatic. The model's atmospheric absorption increased by nearly 30%, the upper troposphere warmed by as much as 4 K, and the strength of the Hadley circulation was reduced by 12%, which resulted in lower surface wind speeds that in turn reduced the surface latent heat flux by 25 W m^{-2}. But despite these changes in model behavior, relative to CCM2, changes in ΔCRF are quite modest, as is demonstrated in Figure 17. A comparable conclusion was reached in a somewhat different context; *Cess et al.* [1996] showed that CCM2 and CCM2A, for an idealized climate change, produced very similar cloud feed-

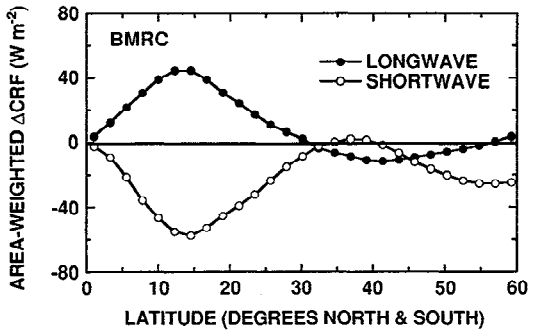

Figure 16. Zonal mean LW and SW ΔCRF for BMRC.

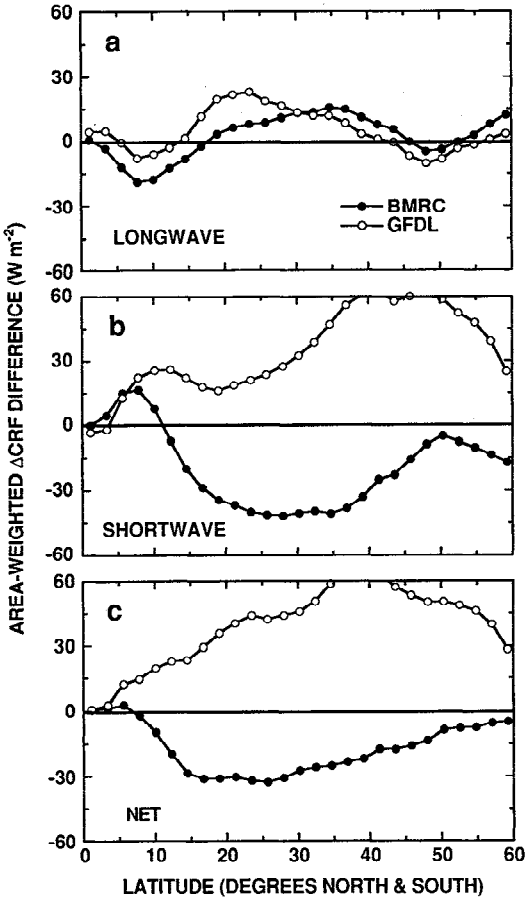

Figure 15. Zonal mean (a) CSIRO versus ERBE, (b) ECHAM versus ERBE, and (c) GFDL versus ERBE differences in net ΔCRF.

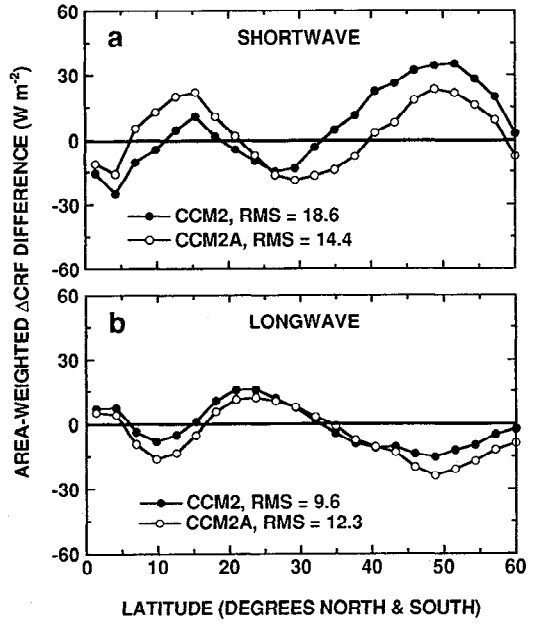

Figure 17. Zonal mean (a) SW and (b) LW ΔCRF for CCM2 and CCM2A.

back, as was also the case for UKMO and a version of that model in which enhanced cloud absorption was likewise incorporated. The interesting point is that cloud feedback constitutes the change in CRF resulting from a change in global climate, while in the present study ΔCRF is the seasonal change in CRF. Thus the inference from both this study and *Cess et al.* [1996] is that a change in CRF, induced either by seasonal change or by global climate change, is quite invariant to the models' SW cloud absorption.

6. Concluding Remarks

Zonal mean ΔCRF (i.e., January minus July and SH minus NH), determined from ERBE data, is primarily driven by seasonal changes of cloud amount. The same conclusion applies to the GCMs. SW CRF is an integrated measure of changes in cloud amount at all altitudes, while LW ΔCRF is more a measure of upper level clouds. Thus comparing both, as generated by GCMs, with ERBE LW and SW ΔCRF provides important insights into seasonal cloud amount variations, as we have demonstrated in the previous section using a subset of the models. Specifically, models that produce greater LW than SW ΔCRF differences, relative to ERBE, most likely are doing a poorer job of replicating seasonal changes in cloud amount for upper level clouds, while the reverse (greater SW differences) suggests a problem with low level clouds. Because of this LW versus SW behavior, some models produce very similar LW ΔCRF, indicating comparable seasonal variations of upper level cloud amounts, but very dissimilar SW ΔCRF caused by low level cloud differences.

A surprising finding of the present study was the latitudinal phasing error associated with ΔCRF, for which seasonal oscillations of zonal cloud patterns extend too far poleward by one latitudinal grid. Ten of the eighteen models exhibit this behavior to varying degrees, and these include all models (six) that use moisture convergence as closure in their convection schemes, raising the possibility that the models' convection schemes may be the cause of this behavior.

Acknowledgments. This study was performed under the auspices of the Environmental Sciences Division of the U.S. Department of Energy. Additional support was provided by the National Aeronautics and Space Administration, the National Science Foundation, the Bundesminister für Forschung and Technologie (Germany), the Programme National d'Etude de la Dynamique du Climat (France), the International Science Foundation, the U.S.-Russian Working Group VIII Activity, and the Commission of European Communities.

References

Barker, H. W., Methodological dependencies of cloud radiative forcing for the Canadian Climate Centre second-generation general circulation model, *J. Geophys. Res.*, *100*, 1017–1025, 1995.

Barker, H. W., S. R. Pal, and A. I. Carswell, Infrared flux transmittances for inhomogeneous cirrus clouds, in *IAMAP International Radiation Symposium*, pp. 145–149, A. Deepak, Hampton, Va., 1993.

Cess, R. D., and G. L. Potter, Exploratory studies of cloud radiative forcing with a general circulation model, *Tellus, Ser. A*, *39*, 460–473, 1987.

Cess, R. D., et al., Intercomparison and interpretation of climate feedback processes in 19 atmospheric general circulation models, *J. Geophys. Res.*, *95*, 16,601–16,615, 1990.

Cess, R. D., E. F. Harrison, P. Minnis, B. R. Barkstrom, V. Ramanathan, and T. Y. Kwon, Interpretation of seasonal cloud-climate interactions using Earth Radiation Budget Experiment data, *J. Geophys. Res.*, *97*, 7613–7617, 1992a.

Cess, R. D., G. L. Potter, W. L. Gates, J.-J. Morcrette, and L. Corsetti, Comparison of general circulation models to Earth Radiation Budget Experiment data: Computation of clear-sky fluxes, *J. Geophys. Res.*, *97*, 20,421–20,426, 1992b.

Cess, R. D., et al., Absorption of solar radiation by clouds: Observations versus models, *Science*, *267*, 496–499, 1995.

Cess, R. D., et al., Cloud feedback in atmospheric general circulation models: An update, *J. Geophys. Res.*, *101*, 12,791–12,794, 1996.

Gates, W. L., AMIP: The Atmospheric Model Intercomparison Project, *Bull. Am. Meteorol. Soc.*, *73*, 1962–1970, 1992.

Harrison, E. F., P. Minnis, B. R. Barkstrom, V. Ramanathan, R. D. Cess, and G. G. Gibson, Seasonal variation of cloud radiative forcing derived from the Earth Radiation Budget Experiment, *J. Geophys. Res.*, *95*, 18,687–18,703, 1990.

Kiehl, J. T., J. J. Hack, M. H. Zhang, and R. D. Cess, Sensitivity of a GCM climate to enhanced shortwave cloud absorption, *J. Clim.*, *8*, 2200–2212, 1995.

Nemesure, S., R. D. Cess, E. G. Dutton, J. J. DeLuisi, Z. Li and H. G. Leighton, Impact of clouds on the shortwave radiation budget of the surface-atmosphere system for snow-covered surfaces, *J. Clim.*, *4*, 579–585, 1994.

Phillips, T. J., A summary documentation of the AMIP models, *Rep. 18*, 343 pp., Program for Clim. Model Diagnosis and Intercomparison, Lawrence Livermore Natl. Lab., Livermore, Calif., 1994.

Pilewskie, P., and F. P. J. Valero, Direct observations of excess solar absorption by clouds, *Science*, *267*, 1626–1629, 1995.

Potter, G. L., J. M. Slingo, J.-J. Morcrette, and L. Corsetti, A modelling perspective on cloud radiative forcing, *J. Geophys. Res.*, *97*, 20,507–20,518, 1992.

Ramanathan, V., R. D. Cess, E. F. Harrison, P. Minnis, B. R. Barkstrom, E. Ahmad, and D. Hartmann, Cloud-radiative forcing and climate: Results from the Earth Radiation Budget Experiment, *Science*, *243*, 57–63, 1989.

Ramanathan, V., B. Subasilar, G. Z. Zhang, W. Conant, R. D. Cess, J. T. Kiehl, H. Grassl, and L. Shi, Warm pool heat budget and shortwave cloud forcing: A missing physics, *Science*, *267*, 499–503, 1995.

Wielicki, B. A., R. D. Cess, M. D. King, D. A. Randall, and E. F. Harrison, Mission to Planet Earth: Role of clouds and radiation in climate, *Bull. Am. Meteorol. Soc.*, *76*, 2125–2153, 1995.

Zhang, M. H., R. D. Cess, T. Y. Kwon, and M. H. Chen, Approaches of comparison clear-sky radiative fluxes from general circulation models with Earth Radiation Budget Experiment data, *J. Geophys. Res.*, *99*, 5515–5523, 1994.

V. Alekseev, V. Dymnikov, V. Galin, and E. M. Volodin, Otdelenie Chislitel'noi Matematiki, Rossiiskaya Akademiya Nauk, 32A Leninskii Prospekt, 117334 Moskva, Russia.

H. W. Barker, Canadian Climate Centre, Downsview, Ontario, Canada M3H 5T4.

S. Bony and H. Le Treut, Laboratoire de Météorologie Dynamique, 24, rue Lhomond, 53231 Paris Cedex 05, France.

R. D. Cess and M. H. Zhang, Institute for Terrestrial and Planetary Atmospheres, Marine Sciences Research Center, State University of New York at Stony Brook, Stony Brook, NY 11794. (e-mail: cess@atmsci.msrc.sunysb.edu)

R. A. Colman, J. R. Fraser, and B. J. McAvaney, Bureau of Meteorology Research Centre, GPO Box 1298, Melbourne, 3001 Victoria, Australia.

D. A. Dazlich, L. D. Fowler, and D. A. Randall, Department of Atmospheric Sciences, Colorado State University, Fort Collins, CO 80523.

A. D. Del Genio and Y. Kim, NASA Goddard Institute for Space Studies, 2880 Broadway, New York, NY 10025.

M. Déqué and B. Timbal, Météo-France, Centre National de Recherches Météorologiques, 42, avenue G. Coriolis, 31057 Toulouse Cedex, France.

M. R. Dix, Division of Atmospheric Research, Commonwealth Scientific and Industrial Research Organisation, Private Bag 1, Aspendale, Victoria 3195, Australia.

M. Esch and E. Roeckner, Max-Planck-Institut für Meteorologie, Bundesstrasse 55, 20146 Hamburg, Federal Republic of Germany.

W. L. Gates, G. L. Potter, and K. E. Taylor, Program for Climate Model Diagnosis and Intercomparison, Lawrence Livermore National Laboratory, Livermore, CA 94550.

J. J. Hack and J. T. Kiehl, National Center for Atmospheric Research, Boulder, CO 80307.

W. J. Ingram, Hadley Centre for Climate Prediction and Research, U.K. Meteorological Office, London Road, Bracknell, Berkshire RG12 2SY, England.

X.-Z. Liang and W. C. Wang, Atmospheric Sciences Research Center, State University of New York at Albany, Albany, NY 12205.

V. P. Meleshko and P. V. Sporyshev, Glavnaya Geofizicheskaya Observatoriya imeni A. I. Voeikova, 7 ulitsa Karbisheva, 194018 Sankt-Peterburg, Russia.

J.-J. Morcrette, European Centre for Medium-Range Weather Forecasts, Reading, Berkshire RG2 9AX, England.

M. E. Schlesinger and W. Wang, Department of Atmospheric Sciences, University of Illinois, Urbana, IL 61801.

R. T. Wetherald, NOAA Geophysical Fluid Dynamics Laboratory, Princeton University, P.O. Box 308, Princeton, NJ 08540.

(Received December 2, 1996; revised March 20, 1997; accepted March 26, 1997.)